CROSS-POLARIZED SYNTHETIC APERTURE RADAR

A New Potential Measurement Technique for Hurricanes

BY BIAO ZHANG AND WILLIAM PERRIE

A new means of retrieving wind measurements from satellite data eliminates need for external wind direction and radar incidence angle inputs and provides linear response at high enough wind speeds for observing hurricanes.

The forecasting of hurricane intensities and tracks is extremely important for the protection of coastal residents and infrastructure. Accurate measurements are important for improving hurricanes forecasts. The first applications of microwave remote sensing technology to hurricanes involved an airborne active scatterometer and passive radiometer during Hurricane Allen, demonstrating their potential for reliable measurements (Jones et al. 1981). Since that time, considerable effort has been devoted to measuring hurricane winds from airborne and spaceborne instruments. For reliable passive microwave measurements of surface winds, the current state-of-the-art instrument is the airborne stepped-frequency microwave radiometer (SFMR) (Uhlhorn and Black 2003). Averaged (10 s) wind speeds from SFMR have been compared with dropwindsonde near-surface estimates and attained 4 m s^{-1} rms error across a range of measured wind speeds, from 10 to 70 m s^{-1} (Uhlhorn et al. 2007). However, although SFMR provides the most reliable measurements of surface winds, it can only provide point measurements along the aircraft flight track.

Wind speeds from synthetic aperture radar (SAR) images are routinely estimated using an empirical geophysical model function (GMF), such as C-band model 4 (CMOD4) (Stoffelen and Anderson 1997) or C-band model 5 (CMOD5) (Hersbach et al. 2007). These GMFs are derived from C-band scatterometer measurements, and they relate wind vectors to the measured normalized radar cross section (NRCS) in VV polarization and the radar incidence angle. Using wind direction and incidence angle as well as the NRCS at the pixel of interest, the associated wind speed can be computed with the GMF mentioned above. Thus far, studies have shown that SAR

AFFILIATIONS: ZHANG—School of Marine Sciences, Nanjing University of Information Science and Technology, Nanjing, China, and Fisheries and Oceans Canada, Bedford Institute of Oceanography, Dartmouth, Nova Scotia, Canada; PERRIE—Fisheries and Oceans Canada, Bedford Institute of Oceanography, Dartmouth, Nova Scotia, Canada
CORRESPONDING AUTHOR: William Perrie, Bedford Institute of Oceanography, 1 Challenger Drive, Dartmouth, NS B2Y 4A2, Canada
E-mail: william.perrie@dfo-mpo.gc.ca

The abstract for this article can be found in this issue, following the table of contents.
DOI:10.1175/BAMS-D-11-00001.1

In final form 30 September 2011

measurements achieve an accuracy of about 1–2 m s^{-1} for low to moderate wind speeds using CMOD4 (Lehner et al. 1998; Horstmann et al. 2003; Monaldo et al. 2004), but they underestimate wind speeds higher than 20 m s^{-1} (Donnelly et al. 1999).

SAR wind speed retrieval accuracy is affected by errors in estimated wind directions. In general, there are three approaches that have been developed to obtain wind directions: 1) use wind-induced streaks visible in the SAR image to infer the wind direction (Gerling 1986; Vachon and Dobson 1996; Horstmann et al. 2005; Reppucci et al. 2010), 2) acquire wind directions from an operational weather prediction system (Monaldo et al. 2001), and 3) obtain wind directions from scatterometer measurements (Xu et al. 2010). However, there are some limitations to acquiring the wind directions from these methods. In approach 1, although useful and convenient, the use of linear features in the SAR image to estimate wind direction can sometimes leads to erroneous results. Wind-induced signatures, such as wind rows, are most conspicuous under unstable atmospheric conditions; but in some cases, especially in neutral or stable conditions, they are not present at all (Monaldo et al. 2001). In addition, there can be other features in SAR images, such as oceanic or atmospheric internal waves, that produce linear features on the same spatial scale as wind rows. These nonwind streak features are not generally aligned with the local wind vectors and can contaminate wind direction retrievals inferred from the SAR image directly. In approach 2, the virtue of using wind directions from meteorological forecast models is that they tend to produce physically reasonable estimates, but the disadvantage is that their spatial resolutions are generally far less than the SAR resolution. Moreover, global weather models do not necessarily include sufficient aspects of marine atmospheric boundary layer physics to resolve the finescale features observed by SAR (Li et al. 2011). Finally, in approach 3, the problem with scatterometer observations is that near coastal regions, there is contamination from land signals (Yang et al. 2011b), and thus we can not get accurate wind directions in these areas.

Conventional optical satellite images are limited in that they can only view hurricanes at the top of the clouds. By comparison, C-band SAR can penetrate cloud and rainbands, to some extent, and therefore uniquely monitor hurricanes from space, with wide swaths and high resolution (Friedman and Li 2000; Katsaros et al. 2002). In recent years, much attention has focused on the retrieval of hurricane winds from C-band *RADARSAT-1* and *Environmental Satellite* (*Envisat*) Advanced Synthetic Aperture Radar (ASAR) images (Horstmann et al. 2005; Shen et al. 2006; Reppucci et al. 2010). Studies show that CMOD5 provides better estimates than those from CMOD4 for hurricane-forced winds (Horstmann et al. 2005). However, wind retrievals from hurricanes using SAR images still face some challenges; for example, CMOD5 generally underestimates the highest estimates for wind speeds (Pichel et al. 2007) due to heavy rain contamination and additional effects associated with severe sea states, which can strongly dampen the NRCS. It is well known that the drag coefficient and sea surface roughness do not continuously increase as surface wind speeds approach and exceed marginal hurricane intensity, >33 m s^{-1}, but asymptote to limiting values (Powell et al. 2003; Donelan et al. 2004). Both airborne C- and Ku-band ocean surface NRCS measurements clearly show that the NRCS in VV polarization does not continue to increase as winds increase beyond marginal hurricane strength (Fernandez et al. 2006). Thus, NRCS saturation creates a wind speed ambiguity problem for SAR wind speed retrievals (Shen et al. 2009). Moreover, in hurricane wind regimes, although the wind direction dependence of the NRCS of CMOD5 is much weaker than that of CMOD4 (Horstmann et al. 2005), inaccurate wind directions are still able to cause wind speed retrieval errors.

It is very important for hurricane forecasters to get the near-real-time, accurate hurricane-forced winds from space. Until now, measurements from spaceborne SAR observations have not been validated for high wind speeds (in the range of >20 m s^{-1}). Recently, C-band cross-polarized ocean backscatter has been documented as being insensitive to the wind direction and the radar incidence angle, and thus can be used to directly retrieve wind speeds (Zhang et al. 2011; Vachon and Wolfe 2011; Hwang et al. 2010). In this paper, we aim to establish a C-band Cross-Polarization Ocean (C-2PO) model with potential application for high (>20 m s^{-1}) wind retrievals. The winds derived from the C-2PO model, and from CMOD5.N (Hersbach 2010), using two *RADARSAT-2* dual-polarization (VV, VH) SAR images acquired over Hurricanes Earl and Ike, are compared with collocated SFMR and in situ buoy measurements, as well as H*Wind data. We show that because C-2PO does not need any external wind directions and radar incidence angles, its retrieval methodology is significantly simplified compared to CMOD5.N. Moreover, in the presently available quad-polarization SAR data, the SAR-observed NRCS in cross polarization linearly increases, even for wind speeds up to 26 m s^{-1}, which suggests that it may be potentially useful in high wind

retrievals in severe storms, such as typical cyclones and hurricanes.

DATASETS. The datasets consist of 1) 1,126 *RADARSAT-2* fine quad-polarization (HH, HV, VH, and VV) mode SAR images and collocated 52 NDBC buoy observations in the Gulf of Alaska, off the East and West Coasts of the United States and the Gulf of Mexico; 2) a *RADARSAT-2* dual-polarization (VV, VH) SAR image acquired over Hurricane Earl at 2259 UTC 2 September 2010, collocating with dataset 3; 3) airborne SFMR measurements through Hurricane Earl during 2230–2330 UTC 2 September 2010; 4) hourly in situ wind observations from NDBC buoy 41001 for Hurricane Earl; 5) a *RADARSAT-2* dual-polarization SAR image acquired over Hurricane Ike in the Gulf of Mexico at 2356 UTC 10 September 2008; and 6) associated H*Wind data for Hurricanes Earl and Ike. The sidebar briefly describes *RADARSAT-2* SAR, its imaging modes, and advantages over other optical sensors.

For *RADARSAT-2* fine quad-polarization mode SAR data, the entire range of incidence angles is between 20° and 49°. For each individual image, the incidence angle range is about 1.5° across a swath of 25 km. The nominal spatial resolutions in azimuth and range are of 5.4 and 8.0 m, respectively. The fine quad-polarization data have a very low noise floor. Interchannel cross talk is corrected in the processor to better than −35 dB, which is appropriate for HV backscatter measurements, without contamination from the HH or VV polarization data (Touzi et al. 2010). However, for Hurricane Earl, the *RADARSAT-2* SAR image is acquired in dual-polarization imaging mode; the incidence angles in the near and far range are 19.4° and 49.4°, respectively. The pixel spacing is 50 m, and the swath is about 500 km × 500 km. Dual-polarization SAR data may have cross-polarization leakage that can bias wind speeds.

The NDBC buoys measure wind speed and direction, averaged over 8-min periods and reported hourly (www.ndbc.noaa.gov/). All buoy data are converted to equivalent neutral winds at 10-m using the Tropical Ocean and Global Atmosphere Coupled Ocean–Atmosphere Response Experiment (TOGA COARE)

RADARSAT-2

RADARSAT-2 is a C-band spaceborne SAR, which was launched on 14 December 2007. It supports all *RADARSAT-1* beam modes, namely single-polarization standard, fine resolution, wide swath, ScanSAR, and extended coverage beams. Moreover, in addition to dual-polarization (VV, VH) SAR modes, new modes include quad-polarization (HH, HV, VH, and VV) imaging capabilities and multilook fine (which has the same resolution as fine but uses four looks) and ultrafine 3-m-resolution models. All modes are available in both left- and right-looking orientations. Figure SB1 shows an illustration of the *RADARSAT-2* satellite.

SAR has been widely used to measure atmospheric and oceanic phenomenon from space because of its high spatial resolution, large area coverage, and its independence of cloud cover. Observed SAR backscatter intensity can be directly related to centimeter-scale surface waves, which are generated primarily by the effects of wind, as the primary driver for change to the ocean surface roughness. For radar backscatter at moderate incident angles (20°–60°), the NRCS is proportional to the spectral density of the surface roughness on scales comparable to the radar wavelength. For this radar incidence angle range and wind speeds below 20 m s^{-1}, the NRCS is typically largest when the wind blows directly toward the radar and decreases to a minimum when the wind direction is orthogonal to the radar look direction. A second smaller maximum in NRCS occurs when the wind blows directly away from the radar.

For a SAR antenna with significant polarization cross talk, it is still possible to retrieve pure quad-polarization observations of HH, HV, VH, and VV with the four corresponding received voltage measurements. However, it is not possible to recover cross-polarization contamination if using single- or dual-polarization SAR data. Dual-polarization *RADARSAT-2* SAR data have cross-polarization leakage, which can give wind speeds that are biased, but *RADARSAT-2* quad-polarization SAR data do not. The fine quad-polarization data have a very low noise floor. Moreover, interchannel cross talk is corrected in the processor to better than −35 dB, which is appropriate for HV backscatter measurements, without contamination from the HH or VV polarization data (Touzi et al. 2010).

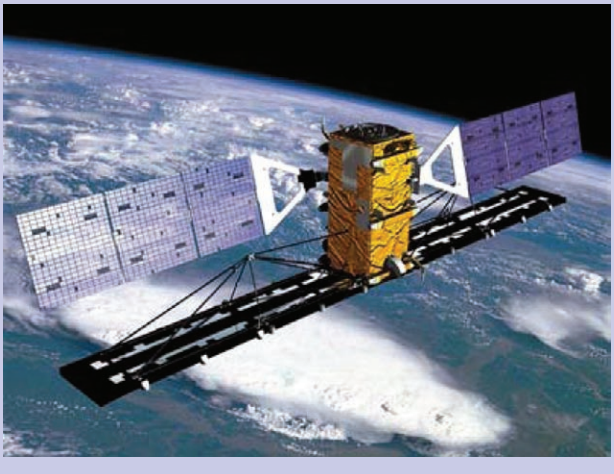

Fig. SB1. Illustration of the *RADARSAT-2* satellite.

bulk flux algorithm (Fairall et al. 2003). Before collocating quad-polarization SAR observations with buoy measurements, we first make a 200 pixel × 200 pixel boxcar average on the NRCS in each polarization, so that the resampled pixel spacing is 1 km. Thus, the area averaged around each buoy is 1 km × 1 km. Finally, the 1,126 NRCS in each polarization, radar incidence angles, and polarization ratios are matched with buoy-measured wind speeds and wind directions.

SFMR measures nadir microwave emissions, expressed in terms of a brightness temperature (T_B) from the sea surface at six C-band frequencies (4.55, 5.06, 5.64, 6.34, 6.96, and 7.22 GHz). A retrieval algorithm uses a geophysical model function relating surface emissivity and wind speed to produce surface wind speed estimates along the flight track (Uhlhorn and Black 2003). On board the National Oceanic and Atmospheric Administration (NOAA) hurricane research aircraft, SFMR data are routinely obtained over tropical cyclones over the Atlantic Ocean in the NOAA Hurricane Research Division (HRD) annual program of research flights. Since 1999, the HRD has transmitted the real-time SFMR surface winds and rainfall rates data (www.aoml.noaa.gov/hrd/data_sub/hurr.html) to the Tropical Prediction Center (TPC) for application to hurricane forecasts. The advantage of SFMR is that it can potentially provide along-track mapping of surface wind speeds and rain rates in relatively high spatial (1.5 km) and temporal (1 Hz) resolutions. The SFMR-derived surface winds are among the most important observations of direct hurricane inner-core surface wind speeds available for TPC forecasters (Black et al. 2011). The SFMR surface wind estimates are well validated by global positioning system (GPS) dropwindsonde measurements (Black et al. 2011; Uhlhorn and Black 2003). Using the latest microwave emissivity–wind speed model function, the SFMR wind speed measurements are within ~4 m s^{-1} rms error of the dropwindsonde-estimated surface wind speeds and within ~5 m s^{-1} of direct 10-m wind speed (U_{10}) measurements (Uhlhorn et al. 2007).

METHODOLOGY. The variations of mean sigma-naught (σ^0) measurements from quad-polarization SAR data with buoy-measured wind speeds at 10 m are shown in Fig. 1. The dataset consists of 1,126 mean σ^0 measurements and collocated wind vector observations from NDBC buoys. Radar incidence angles are between 20° and 49°, wind directions are from 0° to 360°, and wind speeds are from 1 to 26 m s^{-1}. Thus, we show that sigma naught in VV polarization (σ^0_{VV}) depends on radar incidence angle, wind speed, and wind direction (Fig. 1a), which is consistent with σ^0_{VV} variations from accepted CMOD functions. Sigma naught in HH polarization (σ^0_{HH}) shows the same trend but with relatively smaller values (Fig. 1b). However, the behaviors of sigma naught in HV or VH polarizations (σ^0_{HV}, σ^0_{VH}) are significantly different from those of VV or HH polarizations. The former are independent of radar incidence angle and wind direction; however, they are quite dependent on wind speed, at least for wind speeds up to 26 m s^{-1} (Figs. 1c,d). This characteristic indicates that cross-polarized SAR observations can simplify wind speed retrieval from SAR imagery.

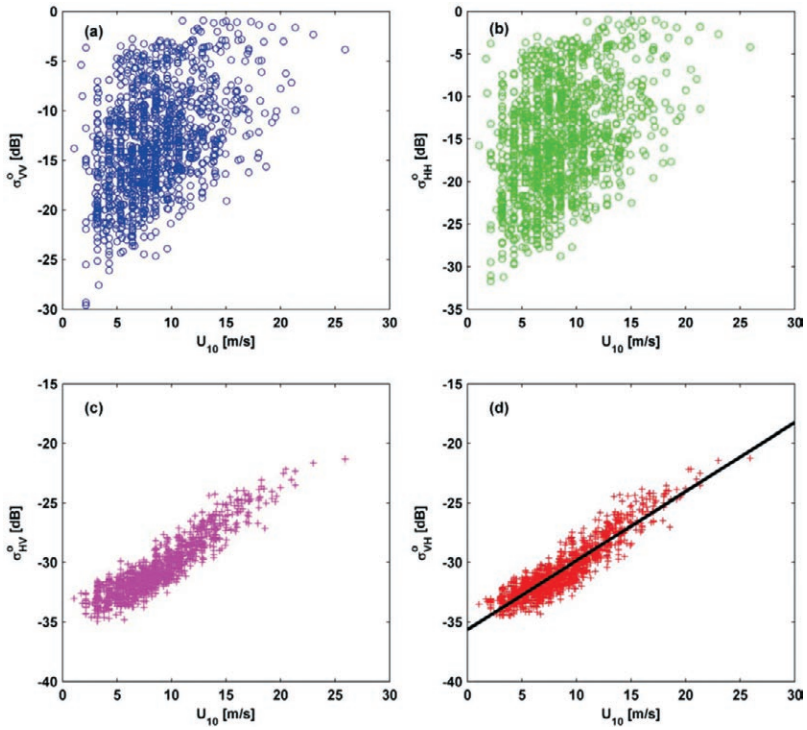

FIG. 1. Mean σ^0 vs in situ buoy-measured U_{10}: (a) VV polarization, (b) HH polarization, (c) HV polarization, (d) VH polarization. The solid line in (d) corresponds to a nonlinear least square fit. The correlation coefficient between *RADARSAT-2* observed σ^0_{VH} and simulated σ^0_{VH} with Eq. (1) is 0.91.

The marine conditions during the SAR–buoy data collection for Figs. 1, 2 consist of all possible cases of short- or long-fetch wind-generated waves, strong wind gradi-

ents, and swell interactions, from storm systems that sometimes extend across basin-scale distances in the Atlantic, Pacific, and Gulf of Mexico. However, Zhang et al. (2011) found that the resulting SAR wind retrieval model outperforms other models. Thus, the presence of strong horizontal wind gradients within wind fields of Hurricanes Earl or Ike is not a dominant issue for wind retrievals, because these wind gradient features and other processes have all been included in the basic data used in the C-2PO algorithm construction, to some extent.

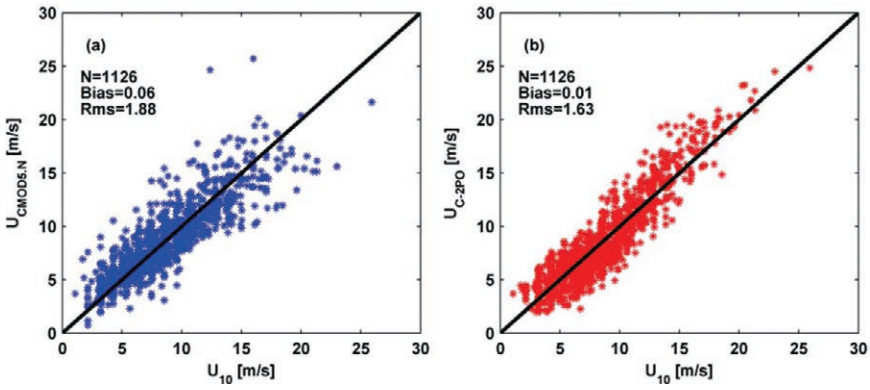

FIG. 2. SAR-retrieved wind speeds from the (a) CMOD5.N model and σ^0_{VV}, and (b) C-2PO model and σ^0_{VH} vs buoy-measured U_{10}.

In general, HV or VH polarizations are induced by volume scattering or by surface tilts (i.e., polarization orientation angle shifts), while VV or HH polarizations are induced by surface scattering; thus, HV or VH polarizations are less correlated with HH and VV polarizations (Lee and Pottier 2009). Phillips (1988) elucidated the double structure of sea surface scatters for radar scattering from the ocean surface. The wind generates a distribution of small slope waves and sporadic steep breaking events. The signature of double structure is in the wind speed dependence of radar returns: linear for scattering from gentle waves and cubic for wave-breaking contributions. Composite Bragg (CB) theory successfully describes the former. The cross-polarization radar return exhibits the typical double structure; its wind speed dependence increases with wind speed from linear to cubic. The enhanced sensitivity of cross-polarization returns in the higher wind data of available measurements suggests that it may be ideal for hurricane wind retrievals.

The highest wind speed observation is 26 m s^{-1} in our datasets of collocated SAR–buoy measurements, shown in Figs. 1 and 2. Thus far, it is interesting to note that we have not seen evidence of backscatter saturation in the available cross-polarized data. We use nonlinear least squares to derive a C-2PO model from Fig. 1d, relating σ^0_{VH} to wind speed at 10-m height (U_{10}). The result is

$$\sigma^0_{VH} = 0.580U_{10} - 35.652. \quad (1)$$

In Eq. (1), the units of σ^0_{VH} and U_{10} are decibel and meters per second, respectively. The correlation coefficient between *RADARSAT-2* observed σ^0_{VH} and simulated σ^0_{VH} with Eq. (1) is 0.91, and the relation does not need external wind direction and radar incidence angle inputs. Thus, C-2PO is a more straightforward mapping of observed NRCS to wind speed compared to CMOD5.N.

To assess the C-2PO model, we compare buoy-measured wind speeds with those from CMOD5.N and C-2PO. For CMOD5.N retrievals, the input wind directions are from buoy observations. The comparisons are shown in Figs. 2a,b. C-2PO has a bias of 0.01 m s^{-1} and an rms error of 1.63 m s^{-1}, and CMOD5.N has a bias of 0.06 m s^{-1} and an rms difference of 1.88 m s^{-1}. Although the wind speed retrieval accuracy of C-2PO is better than that of CMOD5.N for the *RADARSAT-2* quad-polarization SAR data, it still needs to be tested using other C-band SARs, such as *Envisat* ASAR data. Note also that the wind speed retrieval errors existing in CMOD5.N results, induced by inaccurate wind directions, can be avoided by C-2PO. Thus far, our presently available dataset collocating SAR and buoy observations does not include hurricane-forced wind speeds (>33 m s^{-1}). C-2PO needs to be improved by incorporating higher wind observations to allow us to investigate whether this model becomes saturated under hurricane and tropical cyclone conditions.

HURRICANES EARL AND IKE. Analysis of the *RADARSAT-2* dual-polarization (VV, VH) SAR images acquired over Hurricanes Earl and Ike provides an opportunity to compare higher wind retrievals using C-2PO and CMOD5.N. Wind speed retrieval using CMOD5.N does need the wind direction information. Here, we use wind directions from the NOAA HRD wind analysis (H*Wind). These are high-resolution wind analyses provided for tropical cyclones (Powell et al. 1998, 2010). Wind directions from the H*Wind analyses were acquired at 22:30 UTC 2 September 2010, about 29 minutes before *RADARSAT-2* imaging of Hurricane Earl (2259 UTC). The spatial resolution of H*Wind data is

6 km. We first average the SAR data from their original 50-m pixel spacing to 1 km, and then we linearly interpolate the wind directions from H*Wind data to the geographic position of the pixel. Using σ^0_{VV}, and the wind direction and incidence angle at the pixel of interest, we use CMOD5.N to compute the associated wind speed on 1-km scale resolution.

Figures 3a,b show a *RADARSAT-2* SAR image of Hurricane Earl in VV and VH polarization, respectively. Wind speeds for Hurricane Earl from CMOD5.N are shown in the Fig. 3c with overlaid interpolated wind directions from H*Wind. Figure 3d shows the retrieved winds from the C-2PO, without any external wind direction and radar incidence angle inputs. The wind speed resolution is 1 km in Figs. 3c,d. Although it has been documented that CMOD5.N is better than CMOD5 or other GMFs (Hersbach 2010; Zhang et al. 2011), the σ^0_{VV} values predicted by CMOD5.N tend to saturate when wind speed exceeds minimal hurricane force (Shen et al. 2009). However, as shown in Fig. 1d, increasing values for U_{10} correspond to larger σ^0_{VH} values even for wind speeds up to 26 m s^{-1}. As a result, the C-2PO model is better able to reproduce the hurricane eye structure than CMOD5.N, as shown in Figs. 3c,d.

To evaluate the accuracy, we compared the wind speeds from C-2PO and CMOD5.N with those measured by SFMR in Fig. 4a. Winds from C-2PO are shown to be quite consistent with SFMR measurements with a correlation coefficient of 0.80, whereas the CMOD5.N wind speeds are underestimated compared to SFMR values, with a correlation coefficient of 0.52. Scatterplots are presented in Figs. 4b,c. Winds from CMOD5.N have a bias of −4.14 m s^{-1} and an rms error of 6.24 m s^{-1}; whereas for C-2PO winds, the bias and RMS difference are −0.89 and 3.23 m s^{-1}, respectively, which are significant improvements. We can also compare the wind speeds from CMOD5.N and C-2PO with the collocated NDBC buoy 41001 observations. The buoy's measured

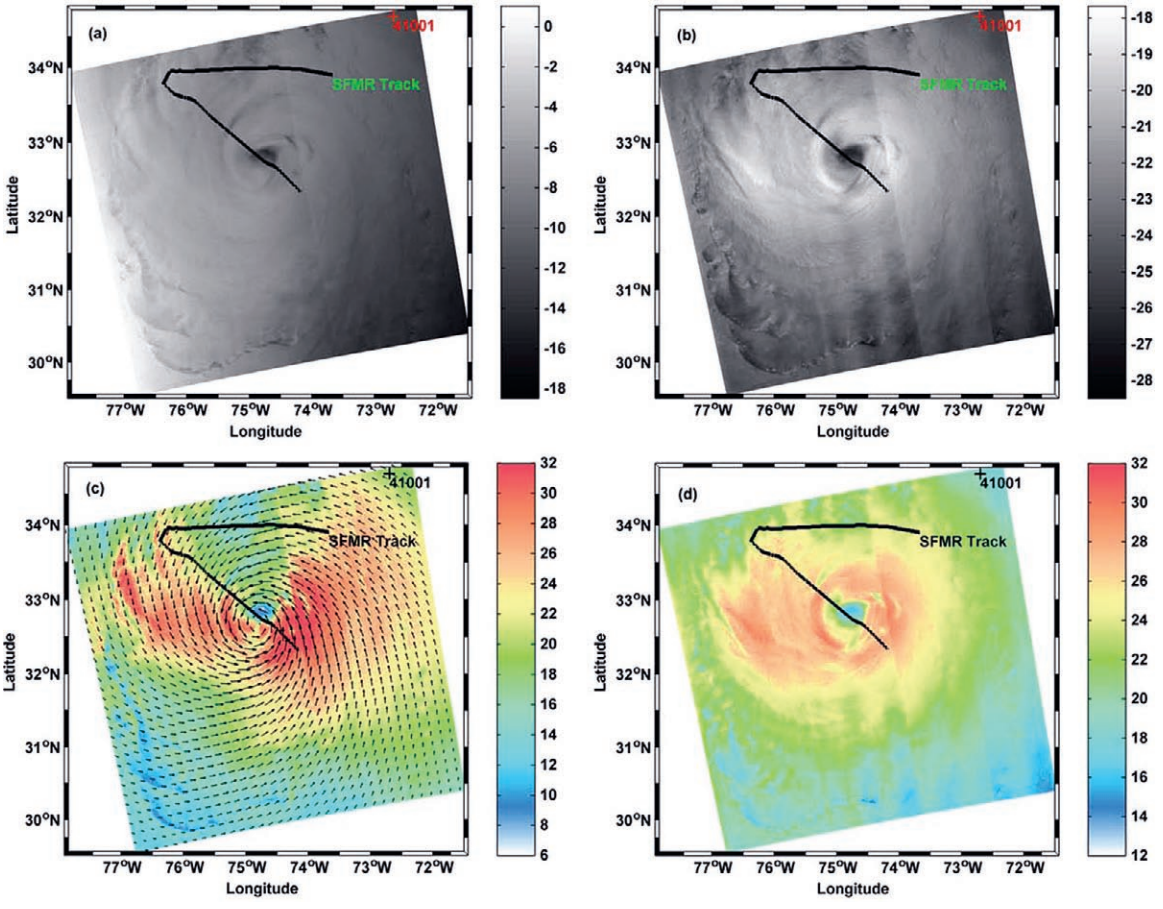

Fig. 3. *RADARSAT-2* dual-polarization SAR image acquired over Hurricane Earl at 2259 UTC 2 Sep 2010: (a) VV polarization and (b) VH polarization, with color bars showing σ^0_{VV} and σ^0_{VH} in dB, respectively. SAR-retrieved wind speeds from the (c) CMOD5.N model and σ^0_{VV}, with external wind directions from NOAA HRD H*Wind overlaid; and (d) C-2PO model and σ^0_{VH}. Color bars showing U_{10} in m s^{-1}. [*RADARSAT-2* data and product from MacDonald, Dettwiler and Associates Ltd.]

10-m wind speed is 18.1 m s^{-1}, whereas the CMOD5.N and C-2PO estimates are 19.5 and 18.7 m s^{-1}, respectively.

In this study, the SFMR rain rate is used to analyze the effect of rain on relatively high (up to ~38 m s^{-1}) wind retrievals from SAR. Measurements of SFMR-retrieved 10-s path-integrated rain rates have been shown to correlate well with airborne radar rainfall measurements (Jiang et al. 2006). Figure 4d shows the SFMR-measured 10-s path-integrated rain rate during 22:30–23:30 UTC 2 September 2010. The heaviest rain rate (34.9 mm h^{-1}) occurred at 23:12 UTC, corresponding to the largest wind speed difference (18.4 m s^{-1}) between the CMOD5.N estimate (16.6 m s^{-1}) and the SFMR (35.0 m s^{-1}) estimates. These large differences might be induced by dampened NRCS values, caused by heavy rain contamination, as well as wave effects and high sea states generated by winds. Additional studies show that for higher winds and σ^0_{VV} values, attenuation is dominant until the rain rate reaches 15 mm h^{-1}, which leads to underestimated wind speeds. For higher rain rates, for example, exceeding 20 mm h^{-1}, the contribution to effective σ^0 from surface backscatter is much smaller than that due to volume scattering by rain. Thus, retrievals of surface wind vectors using σ^0_{VV} under heavy rain conditions are almost impossible without precise knowledge of the rain rate (Tournadre and Quilfen 2003). Moreover, a well-calibrated σ^0_{VV} relation and accurate wind directions are also very important for CMOD5.N. The latter is not needed for C-2PO, as shown in Fig. 3d.

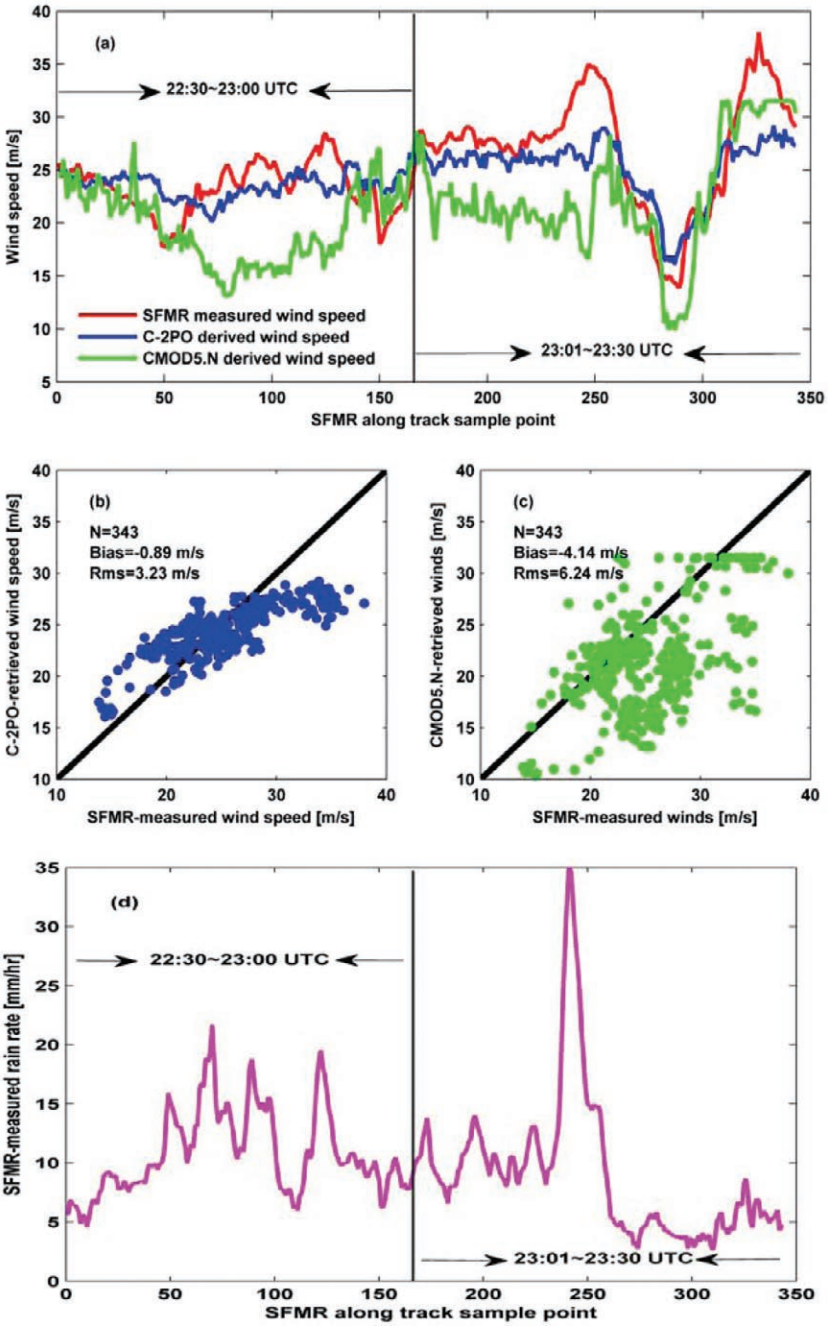

Fig. 4. Comparisons of C-2PO and CMOD5.N SAR-retrieved wind speeds (at 2259 UTC 2 Sep 2010) with collocated SFMR-measured along-track 10-s averaged surface winds during 2230–2330 UTC 2 Sep 2010: (a) time series plot; (b),(c) scatterplots; and (d) SFMR-measured 10-s path-integrated rain rates (mm h^{-1}).

Although C-2PO is a substantial improvement in wind speed retrievals compared to CMOD5.N, it underestimates the highest (28–38 m s^{-1}) winds, shown in Fig. 4b. This bias may be caused by rain-induced cross-polarized NRCS reduction or cross-polarization leakage in dual-polarization SAR data (but not in quad-polarization SAR–buoy data in Figs. 1, 2). There are strong indications that the particular wind conditions characteristic of rainbands

can lead to a reduction in the ocean surface roughness and thus the respective NRCS (Powell 1990). Some studies using scatterometer data have shown that for wind speeds above 30 m s^{-1} and rain rates exceeding 15 mm h^{-1}, the error in the winds can be more than 10 m s^{-1} (Yang et al. 2004). Moreover, the influence of heavy rain on the C-band ocean backscatter has been estimated from an existing radiative transfer model (Reppucci et al. 2008). It was shown that the NRCS attenuation can be more than –1 dB for rain rates of 30 mm h^{-1}, and even larger damping—up to –2 dB—for rain rates of 50 mm h^{-1}. Recent investigations show that for winds of more than 20 m s^{-1}, in storm or hurricane conditions, the 0.5–1-dB NRCS calibration

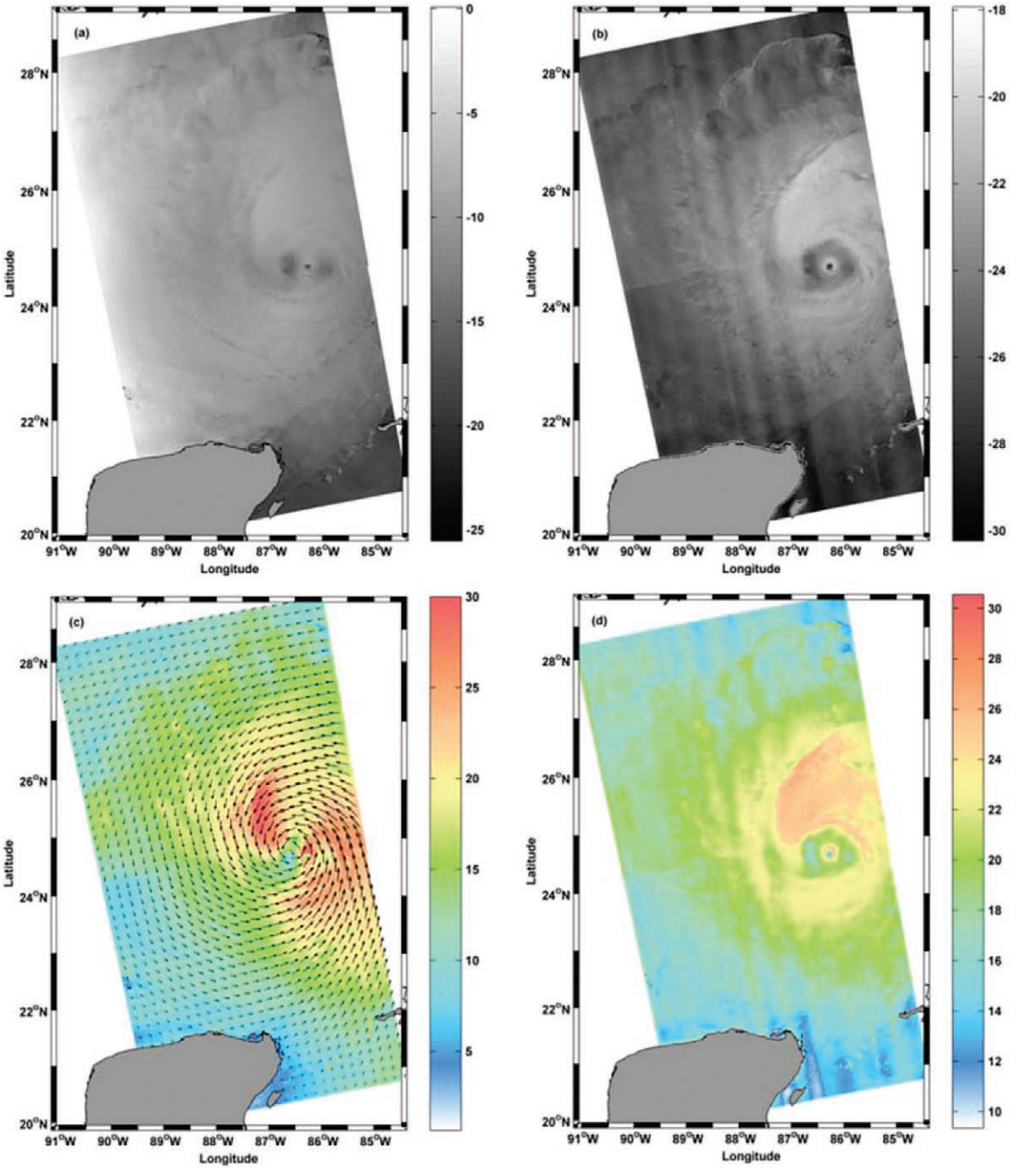

Fig. 5. A *RADARSAT-2* dual-polarization SAR image acquired over Hurricane Ike at 2356 UTC 10 Sep 2008: (a) VV polarization and (b) VH polarization, with color bars showing σ^0_{VV} and σ^0_{VH} in dB, respectively. SAR-retrieved wind speeds from the (c) CMOD5.N model and σ^0_{VV}, with external wind directions from NOAA HRD H*Wind overlaid; and (d) C-2PO model and σ^0_{VH}. Color bars showing U_{10} in m s^{-1}. [*RADARSAT-2* data and product from MacDonald, Dettwiler and Associates Ltd.]

error will induce 3–8 m s^{-1} errors using standard wind retrieval algorithms (Yang et al. 2011a). In addition, *RADARSAT-2* dual-polarization data also suffer from cross-polarization leakage (Touzi et al. 2010), which may result in underestimates in wind speeds.

An additional hurricane example is Hurricane Ike from September 2008. Figures 5a,b show a *RADARSAT-2* dual-polarization SAR image of Hurricane Ike acquired at 23:56 UTC 10 September. Wind speeds for Hurricane Ike from CMOD5.N are shown in Fig. 5c with overlaid interpolated H*Wind wind directions. Wind directions from the H*Wind analyses were acquired at 01:30 UTC 11 September 2008, about 34 minutes after the *RADARSAT-2* imaging of Hurricane Ike. Figure 5d shows the retrieved winds from C-2PO, without any external wind direction and radar incidence angle inputs.

As shown for Hurricane Ike in Figs. 5c,d, the results from C-2PO are better able to reproduce the hurricane eye structure than those of CMOD5.N. For this case study, unfortunately, there are no available SFMR measurements that collocate with the SAR image. To make a quantitative comparison of relative high (up to 38 m s^{-1}) wind retrievals, we compared the wind speeds retrieved from C-2PO and CMOD5.N with those from H*Wind in Figs. 6a,b. Winds from CMOD5.N have a bias of −4.89 m s^{-1} and an rms error of 6.51 m s^{-1}; whereas for C-2PO winds, the bias and rms difference are −0.88 and 4.47 m s^{-1}, respectively.

Thus, the C-2PO model is established from *RADARSAT-2* fine quad-polarization mode SAR data with a low noise floor. One should exercise care when using this model to retrieve relatively high (>20 m s^{-1}) winds from dual-polarization SAR imagery, because the noise floor for dual-polarization data is higher than that for quad-polarization data. Moreover, quad polarization allows the retrieval of cross-channel leakage for antennas of both low and high cross-polarization isolation. However, the cross-channel leakage cannot be retrieved if only single- or dual-polarization measurements are collected, as is the case with the single- or dual-polarization modes of ASAR, *Advanced Land Observing Satellite* (*ALOS*) Phased-Array L-band Synthetic Aperture Radar (PALSAR), *RADARSAT-2*, and TerraSAR-X (Touzi et al. 2010).

SUMMARY. A C-band Cross-Polarization Ocean (C-2PO) model is presented, based on *RADARSAT-2* fine quad-polarization mode SAR measurements. The C-2PO model is insensitive to wind direction and radar incidence angle, and thus it is a straightforward mapping of observed cross-polarized NRCS to wind speed. C-2PO avoids the errors in wind speed retrievals that can occur in CMOD5.N due to errors in wind directions. In presently available quad-polarization data, the observed NRCS in cross polarization increases linearly with wind speed, up to 26 m s^{-1}, which indicates that it could potentially be used to retrieve hurricane winds, including eye structure observations. In comparisons of wind speeds derived from C-2PO and CMOD5.N with buoy data, SFMR measurements, and H*Wind analysis, we show that C-2PO has slightly smaller scatter than CMOD5.N for wind speeds <20 m s^{-1}; for wind speeds in the range of 20– 38 m s^{-1}, the difference in scatter is significant.

In Hurricane Earl, we show the first direct quantitative high wind speed (>20 m s^{-1}) comparisons between spaceborne SAR retrievals and airborne SFMR measurements. Results show that the derived wind speeds from the proposed C-2PO model have

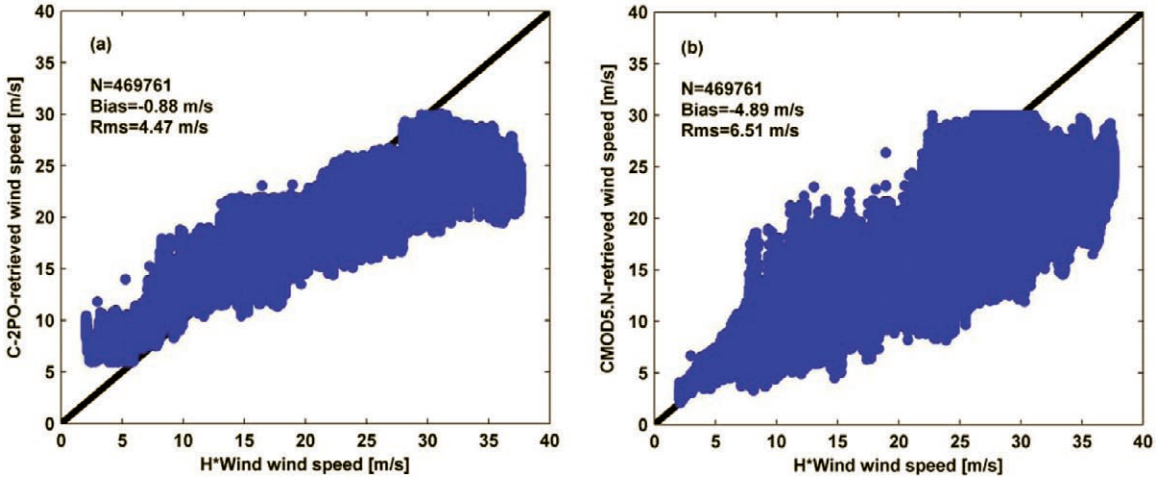

Fig. 6. Comparisons of C-2PO and CMOD5.N SAR-retrieved wind speeds (at 2356 UTC 10 Sep 2008) with collocated H*Wind-derived wind speeds at 0130 UTC 11 Sep 2008.

a bias of −0.89 m s^{-1} and an rms error of 3.23 m s^{-1}, whereas CMOD5.N has a bias of −4.14 m s^{-1} and an rms difference of 6.24 m s^{-1}. Although C-2PO has a smaller wind speed retrieval bias and rms error than CMOD5.N, the two models underestimate relatively high wind speeds (in the range of 30–38 m s^{-1}). The reasons for the underpredictions can be attributed to 1) CMOD5.N being saturated in high winds; 2) co- and cross-polarized NRCS calibration error; 3) CMOD5.N and C-2PO do not account for the rain contamination and effects due to high waves and severe sea states that, for high wind speed (30–38 m s^{-1}) and high rain rate (up to 35 mm h^{-1}), can strongly dampen the NRCS, leading to significant underestimates in wind speeds; and 4) inaccurate wind directions for CMOD5.N.

Ongoing research will include additional high wind observations to improve the C-2PO model and to investigate how to correct the rain effect on NRCS in complicated hurricane sea states. We suggest that C-2PO represents a potential technique for hurricane observations from space. Future C-band RADARSAT Constellation Mission SAR satellites will give SAR data in compact polarization mode with large swath (350 km) and medium resolution (50 m), which can be transformed to quad-polarization data, allowing wind retrievals with C-2PO.

ACKNOWLEDGMENTS. The authors thank the Canadian Space Agency (CSA) for providing *RADARSAT-2* dual- and quad-polarization SAR imagery, and NOAA HRD and NDBC for supplying SFMR and buoy observations, respectively. We also would like to acknowledge the anonymous reviewers for their constructive suggestions, which resulted in substantial improvements to the manuscript. This work is supported by the CSA GRIP projects Building Satellite Data into Fisheries and Oceans Operational Systems and RADARSAT-2 Full Polarization Retrievals of Ocean Waves and Winds and by the National Natural Science Foundation of China project Multi-Frequencies Polarimetric SAR Wind Field Retrieval in Coastal Regions (Grant 41176170).

REFERENCES

Black, P. G., E. Uhlhorn, M. D. Powell, and J. Carswell, cited 2011: A new era in hurricane reconnaissance: Real time measurement of surface wind structure and intensity via microwave remote sensing. [Available online at http://ams.confex.com/ams/last2000/techprogram/paper_12581.htm.]

Donelan, M. A., B. K. Haus, N. Reul, W. J. Plant, M. Stiassnie, H. C. Graber, O. B. Brown, and E. S. Saltzman, 2004: On the limiting aerodynamic roughness of the ocean in very strong winds. *Geophys. Res. Lett.,* **31,** L18306, doi:10.1029/2004GL019460.

Donnelly, W. J., J. R. Carswell, R. E. McIntosh, P. S. Chang, J. Wilkerson, F. Marks, and P. G. Black, 1999: Revised ocean backscatter model at C and Ku band under high-wind conditions. *J. Geophys. Res.,* **104,** 11 485–11 497.

Fairall, C. W., E. F. Bradley, J. E. Hare, and A. A. Grachev, 2003: Bulk parameterization of air–sea fluxes: Updates and verification for the COARE algorithm. *J. Climate,* **16,** 571–591.

Fernandez, D. E., J. R. Carswell, S. Frasier, P. S. Chang, P. G. Black, and F. D. Marks, 2006: Dual-polarized C- and Ku-band ocean backscatter response to hurricane-force winds. *J. Geophys. Res.,* **111,** C08013, doi:10.1029/2005JC003048.

Friedman, K. S., and X. Li, 2000: Monitoring hurricanes over the ocean with wide swath SAR. *Johns Hopkins APL Tech. Dig.,* **21,** 80–85.

Gerling, T. W., 1986: Structure of the surface wind field from the Seasat SAR. *J. Geophys. Res.,* **91,** 2308–2320.

Hersbach, H., 2010: Comparison of C-band scatterometer CMOD5.N equivalent neural winds with ECMWF. *J. Atmos. Oceanic Technol.,* **27,** 721–736.

——, A. Stoffelen, and S. de Haan, 2007: An improved C-band scatterometer ocean geophysical model function: CMOD5. *J. Geophys. Res.,* **112,** C03006, doi:10.1029/2006JC003743.

Horstmann, J., H. Schiller, J. Schulz-Stellenfleth, and S. Lehner, 2003: Global wind speed retrieval from SAR. *IEEE Trans. Geosci. Remote Sens.,* **41,** 2277–2286.

——, D. R. Thompson, F. Monaldo, S. Iris, and H. C. Graber, 2005: Can synthetic aperture radars be used to estimate hurricane force winds? *Geophys. Res. Lett.,* **32,** L22801, doi:10.1029/2005GL023992.

Hwang, P. A., B. Zhang, and W. Perrie, 2010: Depolarized radar return for breaking wave measurements and hurricane wind retrieval. *Geophys. Res. Lett.,* **37,** L01604, doi:10.1029/2009GL041780.

Jiang, H., P. G. Black, E. J. Zipser, F. D. Marks Jr., and E. W. Uhlhorn, 2006: Validation of rain-rate estimation in hurricanes from the stepped frequency microwave radiometer: Algorithm correction and error analysis. *J. Atmos. Sci.,* **63,** 252–267.

Jones, W. L., P. G. Black, V. E. Delnore, and C. T. Swift, 1981: Airborne microwave remote-sensing measurements of Hurricane Allen. *Science,* **214,** 274–280.

Katsaros, K. B., P. W. Vachon, W. T. Liu, and P. G. Black, 2002: Microwave remote sensing of tropical cyclones from space. *J. Oceanogr.,* **58,** 137–151.

Lee, J.-S., and E. Pottier, 2009: *Polarimetric Radar Imaging: From Basics to Applications*. Optical Science and Engineering, Vol. 142, CRC Press, 398 pp.

Lehner, S., J. Horstmann, W. Koch, and W. Rosenthal, 1998: Mesoscale wind measurements using recalibrated ERS SAR images. *J. Geophys. Res.,* **103,** 7847–7856.

Li, X., W. Zheng, X. Yang, Z. Li, and W. G. Pichel, 2011: Sea surface imprints of coastal mountain lee waves imaged by synthetic aperture radar. *J. Geophys. Res.,* **116,** C02014, doi:10.1029/2010JC006643.

Monaldo, F. M., D. R. Thompson, R. C. Beal, W. G. Pichel, and P. Clemente-Colón, 2001: Comparison of SAR-derived wind speed with model predictions and ocean buoy measurements. *IEEE Trans. Geosci. Remote Sens.,* **39,** 2587–2600.

——, ——, W. G. Pichel, and P. Clemente-Colon, 2004: A systematic comparison of QuikSCAT and SAR ocean surface wind speeds. *IEEE Trans. Geosci. Remote Sens.,* **42,** 283–291.

Phillips, O. M., 1988: Radar returns from the sea surface—Bragg scattering and breaking waves. *J. Phys. Oceanogr.,* **18,** 1065–1074.

Pichel, W. G., and Coauthors, 2007: Envisat ASAR applications demonstrations: Alaska SAR demonstration and Gulf of Mexico hurricane studies. *Proc. Envisat Symp.,* Montreus, Switzerland, European Space Agency, 23–27.

Powell, M. D., 1990: Boundary layer structure and dynamics in outer hurricane rainbands. Part I: Mesoscale rainfall and kinematic structure. *Mon. Wea. Rev.,* **118,** 891–917.

——, S. H. Houston, L. R. Amat, and N. Morisseau-Leroy, 1998: The HRD real-time hurricane wind analysis system. *J. Wind Eng. Ind. Aerodyn.,* **77–78,** 53–64.

——, P. J. Vickery, and T. A. Reinhold, 2003: Reduced drag coefficient for high wind speeds in tropical cyclones. *Nature,* **422,** 279–283.

——, and Coauthors, 2010: Reconstruction of Hurricane Katrina's wind fields for storm surge and wave hindcasting. *Ocean Eng.,* **37,** 26–36.

Reppucci, A., S. Lehner, J. Schulz-Stellenfleth, and C. S. Yang, 2008: Extreme wind conditions observed by satellite synthetic aperture radar in the North West Pacific. *Int. J. Remote. Sens.,* **29,** 6129–6144.

——, ——, ——, and S. Brusch, 2010: Tropical cyclone intensity estimated from wide-swath SAR images. *IEEE Trans. Geosci. Remote Sens.,* **48,** 1639–1649.

Shen, H., W. Perrie, and Y. He, 2006: A new hurricane wind retrieval algorithm for SAR images. *Geophys. Res. Lett.,* **33,** L21812, doi:10.1029/2006GL027087.

——, Y. He, and W. Perrie, 2009: Speed ambiguity in hurricane wind retrieval from SAR imagery. *Int. J. Remote Sens.,* **30,** 2827–2836.

Stoffelen, A., and D. Anderson, 1997: Scatterometer data interpretation: Estimation and validation of the transfer function CMOD4. *J. Geophys. Res.,* **102,** 5767–5780.

Tournadre, J., and Y. Quilfen, 2003: Impact of rain cell on scatterometer data: 1. Theory and modeling. *J. Geophys. Res.,* **108,** 3225, doi:10.1029/2002JC001428.

Touzi, R., P. W. Vachon, and J. Wolfe, 2010: Requirement on antenna cross-polarization isolation for the operational use of C-band SAR constellations in maritime surveillance. *IEEE Geosci. Remote Sens. Lett.,* **7,** 861–865.

Uhlhorn, E. W., and P. G. Black, 2003: Verification of remotely sensed sea surface winds in hurricanes. *J. Atmos. Oceanic Technol.,* **20,** 99–116.

——, ——, J. L. Franklin, M. Goodberlet, J. Carswell, and A. S. Goldstein, 2007: Hurricane surface wind measurements from an operational stepped frequency microwave radiometer. *Mon. Wea. Rev.,* **135,** 3070–3085.

Vachon, P. W., and F. W. Dobson, 1996: Validation of wind vector retrieval from ERS-1 SAR images over the ocean. *Global Atmos. Ocean Syst.,* **5,** 177–187.

——, and J. Wolfe, 2011: C-band cross-polarization wind speed retrieval. *IEEE Geosci. Remote Sens. Lett.,* **8,** 456–459.

Xu, Q., H. Lin, X. Li, J. Zuo, Q. Zheng, W. G. Pichel, and Y. Liu, 2010: Assessment of an analytical model for sea surface wind speed retrieval from spaceborne SAR. *Int. J. Remote Sens.,* **31,** 993–1008.

Yang, J., and Coauthors, 2004: Effect of precipitation of ocean wind scatterometry. *Proc. IEEE Int. Geoscience and Remote Sensing Symp.,* Anchorage, Alaska, IEEE, 20–24.

Yang, X., X. Li, W. G. Pichel, and Z. Li, 2011a: Comparison of ocean surface winds from ENVISAT ASAR, MetOp ASCAT scatterometer, buoy measurements, and NOGAPS model. *IEEE Trans. Geosci. Remote Sens.,* **49,** 4743–4750, doi:10.1109/TGRS.2011.2159802.

——, ——, Q. Zheng, X. Gu, W. G. Pichel, and Z. Li, 2011b: Comparison of ocean-surface winds retrieved from QuikSCAT scatterometer and RADARSAT-1 SAR in offshore waters of the U.S. West Coast. *IEEE Geosci. Remote Lett.,* **8,** 163–167, doi:10.1109/LGRS.2010.2053345.

Zhang, B., W. Perrie, and Y. He, 2011: Wind speed retrieval from RADARSAT-2 quad-polarization images using a new polarization ratio model. *J. Geophys. Res.,* **116,** C08008, doi:10.1029/2010JC006522.